Survey and new measurements of turbulent structure near the wall

William W. Willmarth

Department of Aerospace Engineering, The University of Michigan, Ann Arbor, Michigan 48109

Thomas J. Bogar

Department of Physics, Westminister College, New Wilmington, Pennsylvania 16142

A survey of recent measurements of turbulent structure near the wall which are applicable to the phenomenon of drag reduction by polymer additives is presented. Knowledge of the vorticity in the wall region provides a framework for understanding turbulent structure and the effects of polymer additives. New measurements using a small, calibrated streamwise vorticity probe are described. Near the wall where the turbulent production and dissipation are a maximum the streamwise vorticity is a maximum and is highly intermittent. New measurements of the Reynolds stress have also been made with a very small, computer calibrated hot-wire array. Intermittent small scale structures producing rapid oscillations of the hot-wire signals are detected near the wall which are too small to be resolved by the array. Their spatial scale is much less than the Kolmogoroff length. It is suggested that they are associated with streamwise vorticity.

I. INTRODUCTION

The phenomenon of drag reduction by additives (known as the Toms' phenomenon) was reported by Toms[1] in 1948. He observed that the addition of a very small fraction of polymer to a fully turbulent pipe flow of solvent produced a substantial pressure drop below that of the solvent alone at the same flow rate. Since 1948 there have been numerous experimental investigations which provide quantitative information about the Toms' phenomenon in turbulent pipe and boundary layer flows. The effects produced by additives are well documented, but an understanding of the drag reduction mechanism is far from complete.

Lumley[2] reviewed the state of knowledge of drag reduction in 1969 and suggested that additional measurements were needed. The experiments have been found to be extraordinarily difficult because the rheological behavior of the fluid adversely affects the response of pressure and heat transfer probes placed in the flow. A noninvasive technique using the laser-Doppler anemometer has been developed which is now reliable for mean measurements, but still presents serious difficulties for measurements of fluctuating quantities.

The early measurements of Virk *et al.*[3] who used Pitot tubes and hot film sensors were followed by numerous investigations using laser-Doppler anemometers. The measurements reported by Rudd,[4] Reischman and Tiederman,[5] and by Mizushina and Usui in Ref. 6 provide examples of laser-Doppler anemometer measurements. The investigations all indicate that the primary effect of polymer additives during drag reduction in a turbulent flow is located in the region very near the wall where the mean velocity gradient is reduced. This region extends from the wall out to approximately 60 viscous lengths (i.e., $yu_\tau/\nu = y^+ \leq 60$, where u_τ squared is the ratio of wall shear stress to fluid density and ν is the kinematic viscosity). The mean flow and those fluctuating turbulent quantities that have been reliably measured are not significantly affected beyond $y^+ = 60$. This indicates that understanding of the mechanism of drag reduction by additives will require information about the structure of turbulence in the region near the wall.

Many investigations of the structure of wall turbulence in Newtonian fluids have been reported during the past 15 years. Experiments using hot wire probes, wall pressure transducers, and visual methods have produced background information applicable to a better understanding of turbulent structure. The extensive literature and new results have been summarized by Kovasznay,[7,8] Mollo-Christensen,[9] Laufer[10] and Willmarth.[11] In this paper a brief survey of the highlights of the present knowledge of turbulent structure near the wall is presented. Then, recent results that we have obtained in our efforts to measure extremely small scale turbulent structure near the wall are described.

II. SURVEY OF TURBULENT STRUCTURE NEAR THE WALL

A. Vorticity and a model for the intermittent turbulent structure

The essential features of turbulent structure near the wall are reviewed to provide background knowledge necessary for further understanding of the mechanism of drag reduction by additives. Let us begin by mentioning that one of the primary effects of turbulence is to promote mixing in the flow. Consider a boundary layer flow immediately after transition. Turbulent mixing brings high speed fluid very near the wall and carries low speed fluid far from the wall. The result is that the laminar and turbulent mean velocity profiles cross at some point near the wall and that the mean wall shear stress is much larger than the laminar value.

Turbulence in boundary layer or duct flows is self-sustaining and consists of a random distribution of vorticity, ω. The presence of turbulence in the boundary layer produces dramatic changes in the mean vorticity distribution. Figure 1 from Lighthill[12] shows approxi-

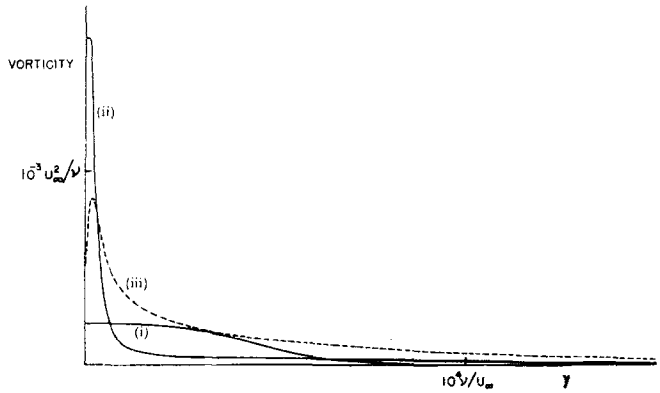

FIG. 1. Distribution of mean vorticity in a boundary layer with uniform external flow: (i) at beginning, (ii) at end of transition. Curve (iii) gives rough values of the root-mean-square vorticity at end of transition. From Lighthill.[12]

mate results from the measurements of Schubauer and Klebanoff.[13] Curve (i) is the laminar distribution of mean vorticity in a boundary layer just before transition at a Reynolds number, Re_x, based on distance, x, from the leading edge of 2.3×10^6. Curve (ii) is the distribution of mean vorticity just after transition at $\mathrm{Re}_x = 3.3\times10^6$. The turbulence has redistributed the vorticity so that at the wall the mean vorticity, τ_w/μ, is many times the laminar value. A small portion (5% of the total) of the mean vorticity is also much farther from the wall in a region of intermittently turbulent flow. Curve (iii) gives approximate values of the root-mean-square vorticity fluctuations in the fully turbulent region after transition. Curve (iii) was apparently deduced by Lighthill from the relation for isotropic turbulence, $\overline{\omega^2} = \epsilon/\nu$, using Schubauer and Klebanoff's[13] measurements of the dissipation, ϵ. Later in the paper accurate measurements of the streamwise component of vorticity are described. The streamwise vorticity fluctuations attain a high maximum very close to the wall near the edge of the sublayer, where turbulent production and dissipation are also a maximum, and extend to the outer edge of the boundary layer.

It is remarkable that turbulence near the wall is able to maintain large gradients of mean and fluctuating vorticity in spite of the large viscous diffusion down the gradient. The processes that accomplish this are central to an understanding of the structure of wall turbulence and the mechanism of drag reduction produced by additives.

The vorticity in a Newtonian fluid obeys the equation

$$\partial\omega/\partial t + (\mathbf{q}\cdot\nabla)\boldsymbol{\omega} = (\boldsymbol{\omega}\cdot\nabla)\mathbf{q} + \nu\nabla^2\boldsymbol{\omega}, \tag{1}$$

which states that the time rate of change of vorticity as one follows the fluid is produced by a nonlinear stretching (or contraction) of existing vorticity, $(\boldsymbol{\omega}\cdot\nabla)\mathbf{q}$, plus diffusion of vorticity, $\nu\nabla^2\boldsymbol{\omega}$. Lighthill[12] has discussed the fact that the wall itself is a source of vorticity. If one considers a flow in the x direction over a plane surface (the x, z plane) with pressure gradients in the x direction, the requirement of no slip at the wall and the Navier Stokes equations plus Eq. (1) yield the flow of z vorticity out of the surface[12]

$$-\nu\frac{\partial\omega_z}{\partial y} = \frac{1}{\rho}\frac{\partial p}{\partial x}, \tag{2}$$

where p is the pressure. The meaning of (2) is that the pressure gradient along a wall creates vorticity tangential to the surface in the direction of the surface isobars. The sense of rotation is that of a ball rolling down the line of steepest pressure fall and the magnitude of the vorticity source strength per unit area $(-\nu\,\partial\omega_z/\partial y)$ is $1/\rho$ times the pressure gradient.

The new vorticity tangential to the wall that is produced by mean and fluctuating wall pressure gradients is eligible for further modification in accordance with Eq. (1). The problem is highly nonlinear because the rotational part of the velocity field appearing in Eq. (1) is "induced" by the vorticity. The induced velocity field alters the vorticity, see Eq. (1), by convection, $(\mathbf{q}\cdot\nabla)\boldsymbol{\omega}$, and stretching, $(\boldsymbol{\omega}\cdot\nabla)\mathbf{q}$. The source of vorticity at the wall also provides a mechanism by which the outer flow in the boundary layer can influence the flow near the wall.

The concept of the wall as a source of vorticity, Eq. (2), which is produced by pressure gradients and then evolves in accordance with Eq. (1) provides a useful framework for further understanding of turbulent structure. Observations of this structure during the past decade using various methods of flow visualization have greatly stimulated turbulence research. Observations of the flow in the sublayer using dye injection methods by Hama and by Beatty *et al.* (see Corrsin[14]) revealed a strong orientation of the dye into streamwise filaments. Later, Kline *et al.*[15] used hydrogen bubbles produced by electrolysis at the surface of a fine wire to observe these filaments of alternating high and low speed flow in the sublayer. Figure 2 is a good example of what they have called the "streaky" sublayer structure. The filaments of increased bubble concentration in the low speed flow regions (the streaks) occur with an average transverse spacing of the order of 100 viscous lengths $(100\nu/u_\tau)$.

Two-point correlation measurements of the sublayer structure using hot wires have been made by Gupta *et al.*[16] They showed that the streaky structure occurs intermittently in space and time and observed alternating large positive and negative transverse spatial correlations with a wavelength of approximately 100 viscous lengths $(\lambda^+ = 100)$ during short time periods. Over longer time periods the two-point correlations with wavelength $(\lambda^+ = 100)$ were completely smeared out by the randomness of the streaky sublayer structure.

Kline and his colleagues[15,17] also observed a recurring coherent pattern of events in the flow near the wall. The pattern of events consisted of a process of gradual lift up and rapid ejection in which low speed fluid containing sublayer streaks moved rapidly away from the wall. Figure 3 is an example of this process and shows a typical lift up and subsequent rapid ejection and contortion of a streak of dye previously injected into the sublayer of a fully turbulent boundary layer.[15] The intermittent process of lift up and contortion of the sublayer fluid was observed to occur randomly in space and

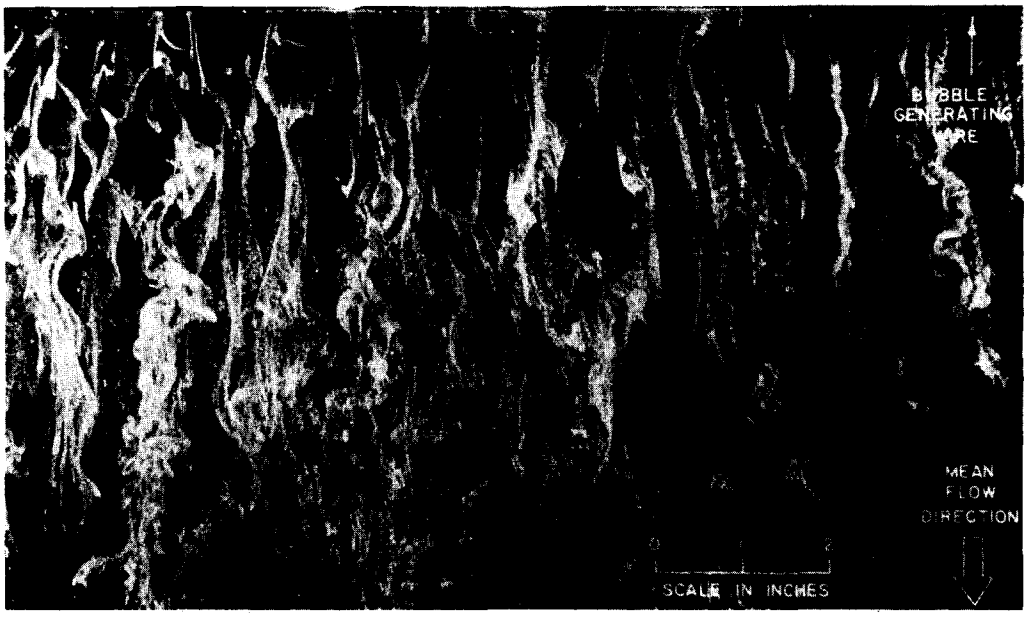

FIG. 2. Photograph of hydrogen bubbles in the sublayer showing "streaky" structure. Bubble generating wire parallel to wall at $y^+ = 8$. From Kline *et al.*[15]

time. Figure 4 shows the averaged trajectories of the ejected fluid obtained from motion pictures of many occurrences of the ejection process. Kim *et al.*[17] have termed the ejection process "bursting" probably because the process appears to be quite rapid. Corrsin has pointed out that in 1957[14]; he used the term "burst" to describe the sudden increases in streamwise velocity accompanied by higher frequencies that were observed intermittently in the oscillograms of streamwise velocity measured by Ruetenik and Corrsin in a turbulent channel flow.

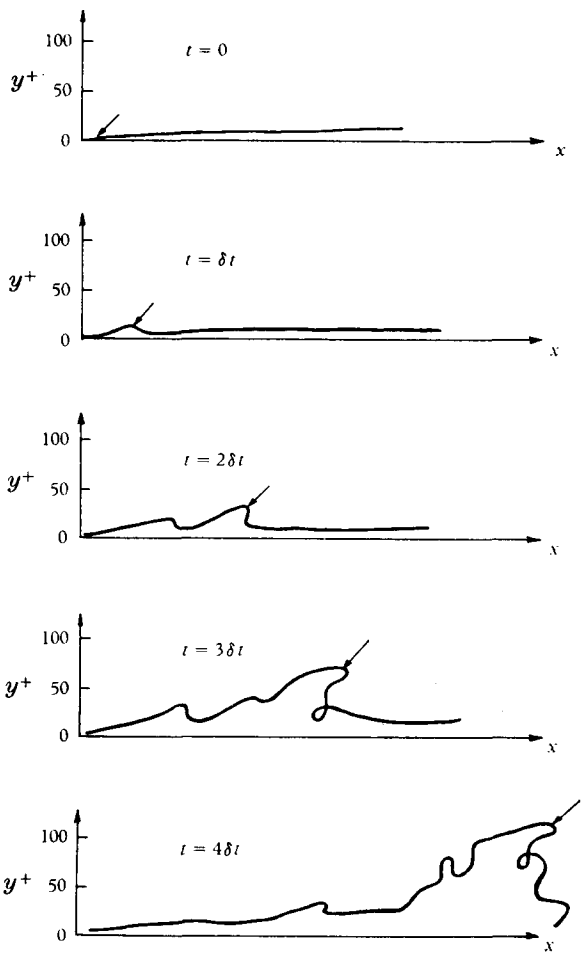

FIG. 3. Dye streak breakup during bursting; illustration as seen in side view. From Kline *et al.*[15]

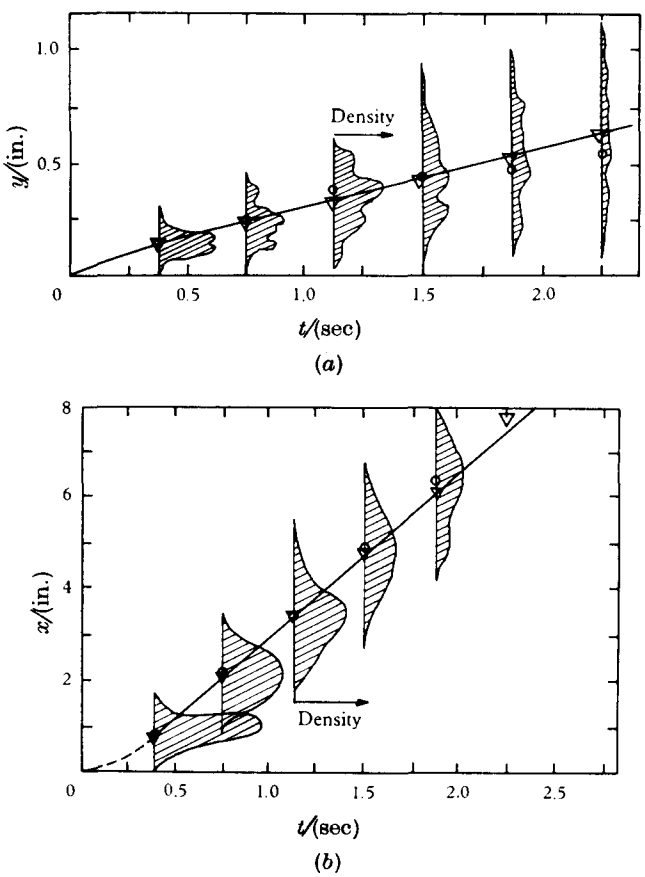

FIG. 4. Trajectories of ejected eddies during bursting, zero pressure gradient. From Kline *et al.*[15]

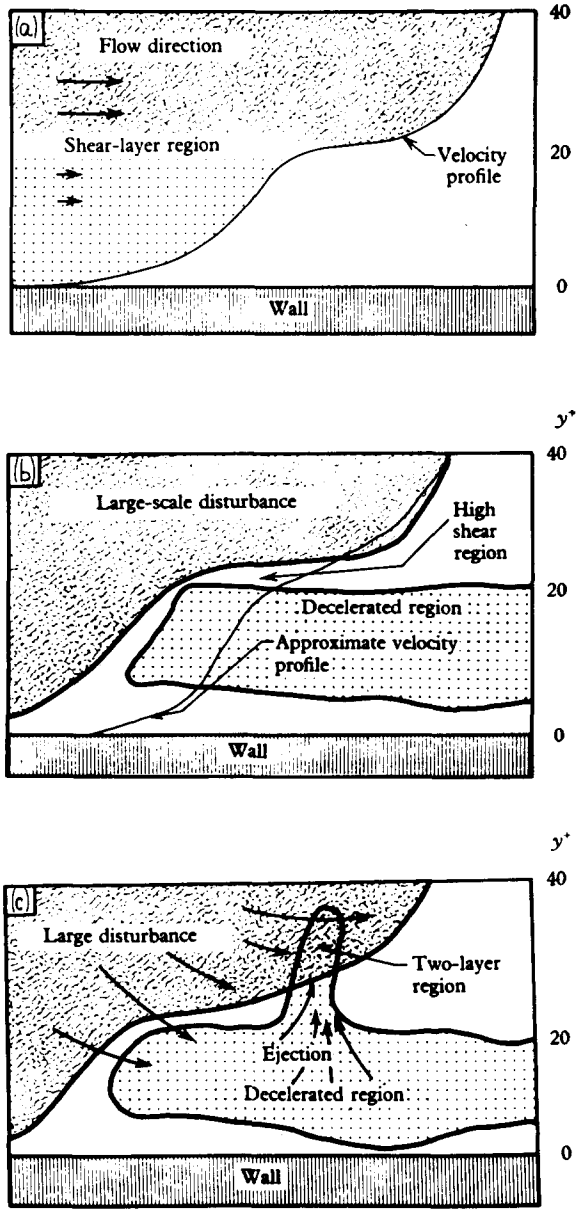

FIG. 5. Sketch of a cross-sectional view of the flow during bursting: (a) formation of low speed region near wall, (b) entrance of large-scale disturbance, (c) ejection and two-layer velocity region. From Corrino and Brodkey.[18]

Kline and his colleagues have also studied bursts using motion pictures of the trajectories of hydrogen bubbles generated on fine wires both normal and parallel to the wall.[17] From frame by frame analysis of the trajectories of periodically generated bubbles (used to determine u and v), they concluded that in the region $0 < y^+ < 100$ essentially all the turbulence production occurs during bursting. They also observed that during gradual lift up of low-speed streaks from the sublayer, unstable (inflectional) instantaneous velocity profiles were formed. These results and observations were substantiated by Brodkey and his colleagues who reported visual studies using motion pictures of the trajectories of very small particles suspended in the flow near the wall. The sequence of events before and after chaotic breakdown during the bursting process as reported by Corino and Brodkey[18] began with the formation of a low speed parcel of fluid near the wall in the region $y^+ \leq 30$. After formation of a low speed region a much larger high-speed parcel of fluid came into view and by "interaction" began to accelerate the low speed fluid. Following this a small scale process of rapid ejection began in which the low speed fluid appeared to be ejected upward with intense, abrupt, and chaotic movements. This sequence of events is sketched in Fig. 5.

The ejection phase ended with the entry from farther upstream of fluid directed primarily in the stream direc- with a velocity approximating the normal mean velocity profile. The entering high-speed fluid carried away the retarded fluid remaining from the ejecting process; this was called the sweep event. Both Corino and Brodkey[18] and Kim *et al.*[17] agree that the bursting phenomenon is an important process for turbulent energy production. Corino and Brodkey concluded that 70% of the Reynolds stress was produced during ejections.

Offen and Kline[19] also reported visual studies of bursting by photography of the flow near the wall using a combination of dye injection at various distances from the wall and hydrogen bubbles generated on a fine wire normal to the wall. They concluded that the severe flow disturbances near the wall that had been observed in previous work[15,17] were associated with just one type of flow structure, a stretched and lifted vortex described by Kline *et al.*[15] in 1967. Figure 6 from Kline *et al.*[15] is a sketch of this intermittently occurring flow structure. The visual observations of Corino and Brodkey are not contradicted by the model and may be visualized as randomly occurring streamwise views of a cross section of the burst sequence of Fig. 6.

The occurrence of a vortex structure in turbulence is hardly a new idea. In 1952 Theodorsen[20] proposed and sketched a "horse shoe" vortex model for the mechanism of turbulent transfer of momentum and heat. A vortex model for the flow near the wall similar to Fig. 6 and evidence supporting it was also reported in 1967 by Willmarth and Tu.[21] They measured spatial correlations between wall pressure fluctuations and the transverse velocity fluctuations in planes normal to the wall and downstream of the wall pressure transducer. The

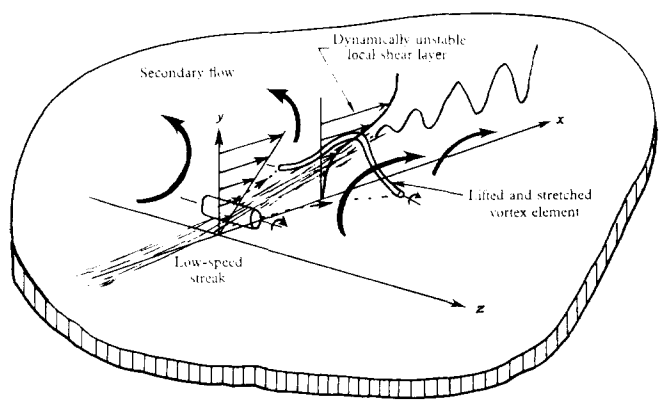

FIG. 6. The model of streak breakup that precedes bursting. From Kline *et al.*[15]

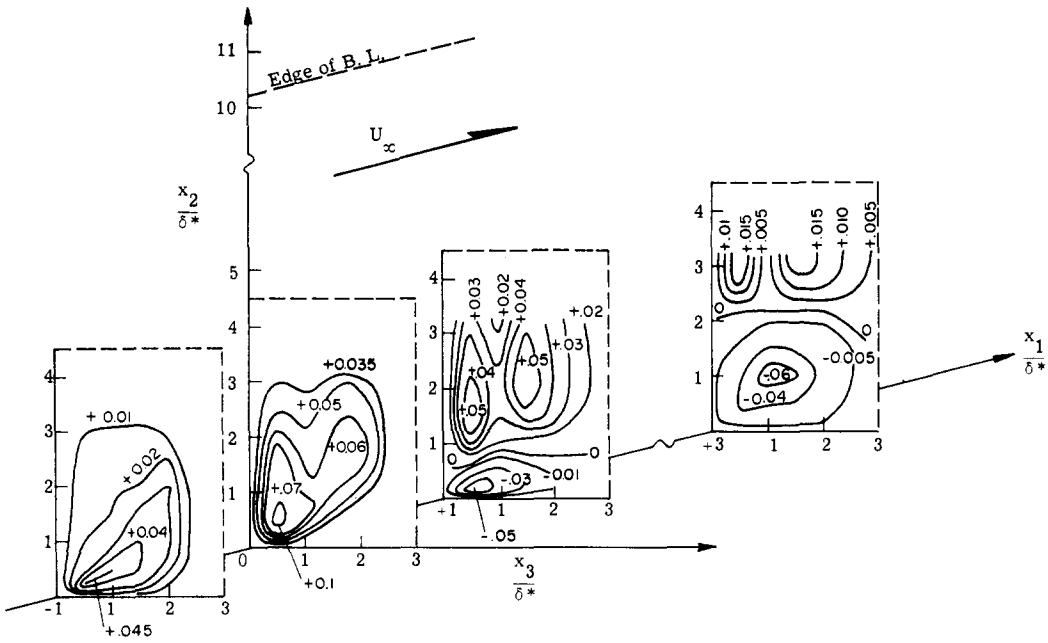

FIG. 7. Three-dimensional diagram of contours of constant wall pressure-spanswise velocity correlation coefficient (R_{pw} = const). From Willmarth and Tu.[21]

results are displayed in Fig. 7 and show the lift up with downstream distance of what must have been streamwise vorticity emanating from the wall. The vorticity produced a reversal of spanwise velocity and hence the sign of $\overline{pw}$ across the inclined plane of zero correlation.

Recently, Kastrinakis *et al.*[22] have reported measurements of streamwise vorticity fluctuations using very small, precisely constructed and calibrated hot wire arrays that can be placed very near the wall of a channel flow. The typical length of the wires and their spacing was 2 to 3 viscous lengths. Figure 8 shows an example of the intermittent nature of the streamwise vorticity and velocity fluctuations at $y^+ = 15$. Notice that the vorticity fluctuations are much more intermittent than the velocity fluctuations. In Figs. 9 and 10 the distribution of the root-mean-square and kurtosis of the streamwise vorticity is displayed. The kurtosis is large, of the order of 6, all across the channel. The root-mean-square vorticity attains a large maximum value of the order of one quarter of the mean wall vorticity at $y^+ \simeq 21$. This indicates the presence of large streamwise vorticity at the same distance from the wall that lift up followed by ejection occur in the model shown in Fig. 6. This is also the region in which turbulent energy production and dissipation are a maximum.

There are numerous measurements and observations by other investigators (see the reviews[7–11] mentioned earlier) which support a model of an intermittently occurring vortical structure near the wall that is responsible for a large fraction of the observed Reynolds stress and turbulence production. Owing to the difficulty of the measurements the model is in a primitive state. Little more than has been described here is known about the structure of the flow field which is produced during bursting near the wall.

B. Evidence of small scale phenomena associated with turbulent structure

One of the primary difficulties presented by measurements of the structure of wall turbulence is the small scale of the turbulent fluctuations. There is considerable evidence (new results will be described in the next section) that the turbulent structure near the wall is of a much smaller scale than the size of probes used in its investigation. Corino and Brodkey[18] in their visual studies of fluid motions near the wall observed a two-layer phenomenon in which groups of particles were observed moving in different directions within a thin illuminated plane of fluid oriented parallel to the stream and normal to the wall. A sketch based on photographs of this phenomenon is shown in Fig. 5(c). The photographs[18] had a depth of field of the order of 20 viscous lengths. The two-layer phenomenon was commonly observed during bursting and this is direct evidence that severe velocity variations within a distance of less than

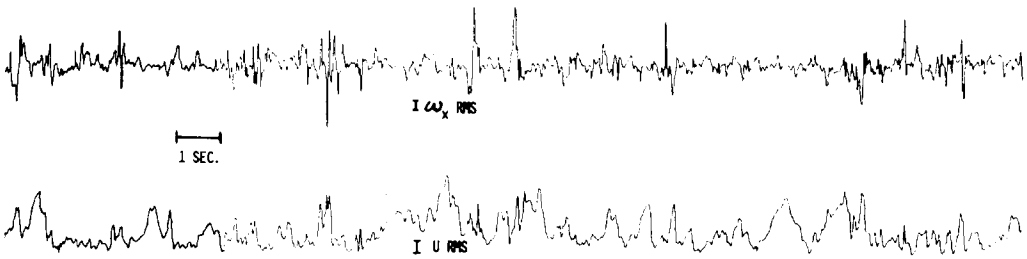

FIG. 8. Record of streamwise vorticity (upper trace) and streamwise velocity (lower trace) as function of time. Probe in fully developed channel flow at $y^+ = 31$. From Kastrinakis *et al.*[22]

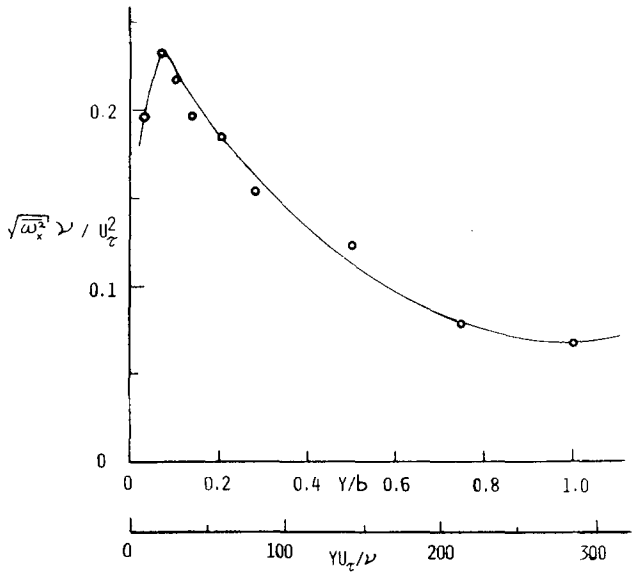

FIG. 9. Root-mean-square streamwise vorticity in a fully turbulent channel flow, channel width is $2b$. From Kastrinakis *et al.*[22]

20 viscous lengths are common during bursting.

Additional observations indicating that the structure of turbulence near the wall is of extremely small scale have been obtained from measurements of wall pressure fluctuations. Emmerling *et al.*[23] performed an experiment in which a section of the wall of an acoustically quiet and vibration free wind tunnel was used as one of the mirrors of a Michelson interferometer. The pressure fluctuations within the boundary layer deflected the mirror surface which was a thin reflecting membrane that covered an array of closely spaced holes drilled in the wall. Motion pictures of the fringe shift patterns on the membrane were analyzed to obtain instantaneous patterns of the wall pressure fluctuations. Figure 11 is an example of a sequence of four frames in which an intense small scale increase in pressure is observed to form and move downstream.

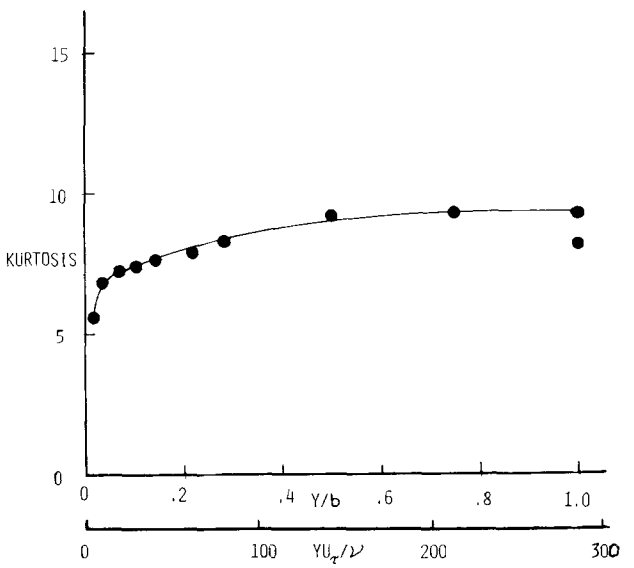

FIG. 10. Kurtosis of streamwise vorticity in a fully turbulent channel flow, channel width is $2b$. From Kastrinakis *et al.*[22]

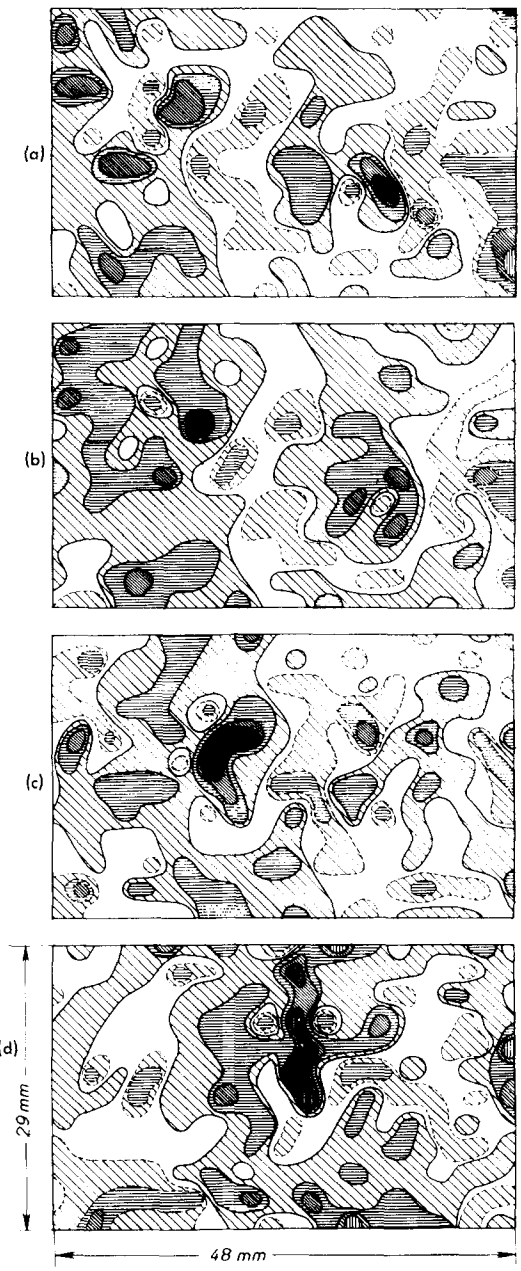

FIG. 11. Contours of instantaneous pressure fluctuations. The darker shading indicates large pressure changes. Positive fluctuations are outlined with solid lines and negative fluctuations with dashed lines. Stream velocity is from left to right. Time increases from (a) to (d): first frame (a) time = 17.57 msec; (b) time = 18 msec; (c) time = 19.14 msec;, (d) time = 20.85 msec. From Emmerling.[23]

The smallest scale of the pressure fluctuations observable in these measurements was limited by the diameter (55 viscous lengths) of the holes drilled in the wall. On some occasions large reversals in the pressure fluctuations could be observed on the membrane surface over a single hole (during pressure reversals the fringes became "S" shaped). This indicates that the transverse scale of the pressure fluctuations is less than half the membrane diameter.

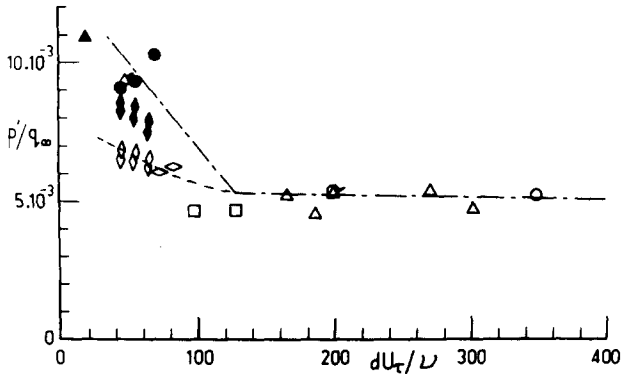

FIG. 12. Variation of measured rms wall pressure fluctuation with transducer size and type. Pinhole data: ●, Blake; ▲, Emmerling[23]; ♦, Bull and Thomas[24] flush-mounted-piezoelectric data: ◇, Lim; ○, Willmarth and Roos; △ Bull; □, Schloemer:, ◊, Bull and Thomas[24]; ▵, Emmerling[23] flush mounted capacitor microphone. From Bull and Thomas.[24]

Further evidence supporting the existence of intense small scale pressure fluctuations was obtained from the results of measurements by a number of investigators of wall pressure fluctuations using small "pinhole" microphones. Figure 12 shows the results of these measurements as summarized by Bull and Thomas.[24] Notice that for pinhole diameters less than 100 viscous lengths there is a dramatic increase in the root-mean-square wall pressure. Bull and Thomas[24] have shown that part of this increase is produced by the discontinuity in the surface caused by the pinhole. The open symbols in Fig. 12 show that the smaller, correct, values measured by very small flush transducers are of the order of 50% higher than the value at $d^+ \simeq 100$. This indicates that the smaller scale wall pressure fluctuations (with scales less than 100 viscous lengths) are of comparable intensity to those of larger scales. (The addition of two uncorrelated random signals of equal strength will result in an increase in the root-mean-square of their sum by a factor of $\sqrt{2}$.)

The wall pressure fluctuations must satisfy Poisson's equation (obtained from the divergence of the momemtum equation)

$$\partial^2(P+p)/\partial x_i^2 = -\rho\partial^2[(U_i+u_i)(U_j+u_j)]/\partial x_i\,\partial x_j. \qquad (3)$$

The velocity gradient terms on the right-hand side of Eq. (3) can be regarded as the source terms in an integral representation for the pressure fluctuations in the flow. It is clear that the pressure at one point is produced by velocity contributions at many others and that the intensity of the pressure fluctuations must die off rapidly with distance from discrete sources. This suggests that the intense small scale wall pressure fluctuations must be produced very near the wall by equally intense and perhaps smaller scale velocity fluctuations. Further knowledge of these small scale flow fluctuations is necessary for a better understanding of the mechanism of drag reduction effects produced by additives.

III. NEW MEASUREMENTS OF SMALL SCALE STRUCTURE USING HOT WIRES

The evidence described here for the existence of small scale flow phenomena near the wall led us to develop an extremely small hot wire array. We have constructed an "X" hot wire array, for measurements of the u and v velocities and the Reynolds stress, that has typical dimensions (wire length and spacing) of 100 μ (approximately 2.5 viscous lengths). The hot wire array was constructed from Wollaston wire with a core of 90% platinum–10% rhodium and a nominal diameter of 0.5 μ. The tapered wire supports were formed by etching the silver coating of the Wollaston wire as described by Bogar.[25] The X array was so small that it could not be made with a precisely aligned and oriented arrangement of the hot wires. To compensate for the lack of precision of the X array geometry a unique calibration scheme that will be described was developed to interpret the two electrical signals produced by the hot wire array. Figure 13 is a photograph of the probe and Fig. 14 is a drawing of the probe showing it positioned near the wall.

The hot wires were operated at 50% overheat. This required only a few milliamperes and was supplied by specially constructed constant temperature hot wire anemometer circuits patterned after the circuit described by Wyngaard and Lumley.[26] The frequency response of the hot-wire anemometer system was uniform up to frequencies of 20 kHz. This was determined by exposing the wires to an intense acoustical sound field.[25] The calibration of the array for the combined response to u and v velocities was accomplished with the aid of a digital computer. The probe to be calibrated was mounted on a mechanical device which slowly pitched it through angles of $\pm 75°$ in the free stream flow in the wind tunnel. A potentiometer was used to measure the pitch angle, θ, of the probe and a propellor anemometer

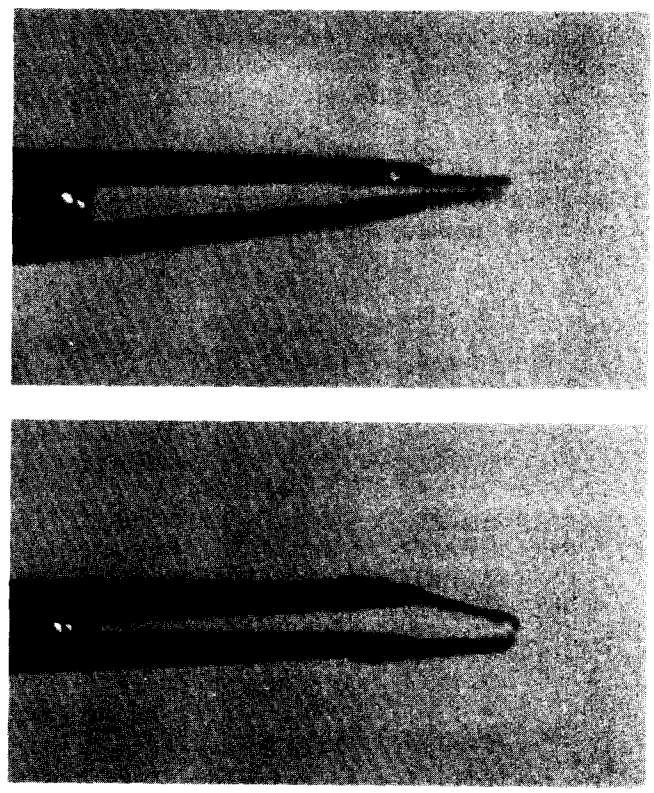

FIG. 13. Small X probe. Photographs of top and side view.

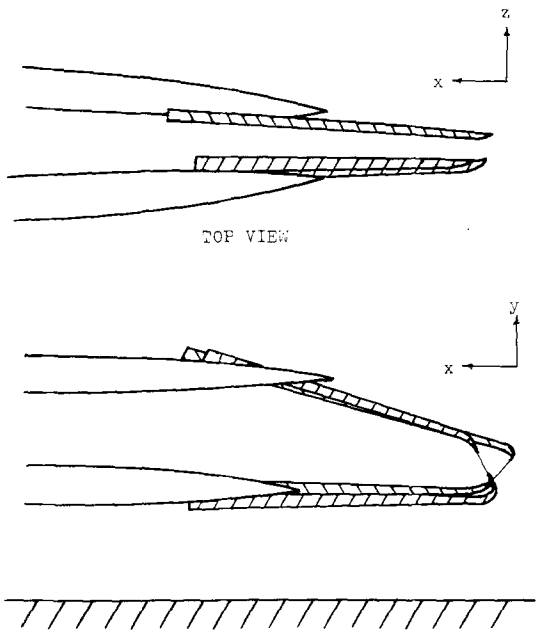

FIG. 14. Small X probe. Drawing of sensitive region; top and side view.

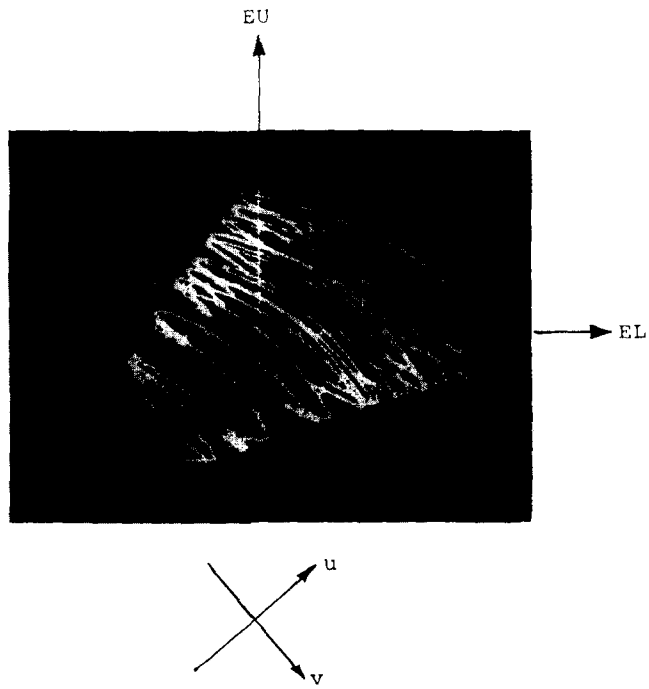

FIG. 16. Photograph of variation of voltages EL and EU displayed on a screen of storage oscilloscope during calibration for turbulence measurements at $y^+ = 335$.

(R. M. Young Co.) was used to measure the mean-free-stream speed in the tunnel. The voltage outputs of the constant temperature anemometers and the voltage corresponding to the pitch angle of the probe and the free stream speed were then recorded on magnetic tape using a frequency modulated system (Honeywell 5600C). As the voltage signals were recorded the pitch angle of the probe was varied periodically and the free stream speed was slowly decreased from speeds greater than any encountered in the boundary layer to zero speed. In this way a record of the probe response was obtained when it was exposed to every possible combination of u and v velocities obtainable in the spatially uniform calibration flow.

The notation for the probe geometry during calibration is shown in Fig. 15. The output voltages from the two hot wires are denoted by EL and EU. The calibration of the X wire makes use of the concept that there is a unique pair of voltages EL and EU for each velocity pair u and v. This is true when the velocity is uniform over the X wires, the spanwise velocity is zero, and the velocity vector lies within the angle, α, formed either by the normals to the two wires or by the two wires themselves, whichever angle is the smaller. In Fig. 15 the angle, α, is that between the normals to the two wires. Obviously, α, is a maximum of 90° when the wires are ideally oriented at right angles. If the inclination of the velocity vector exceeds the range denoted by, α, the wires will produce a nonunique voltage pair that corresponds to more than one velocity pair.

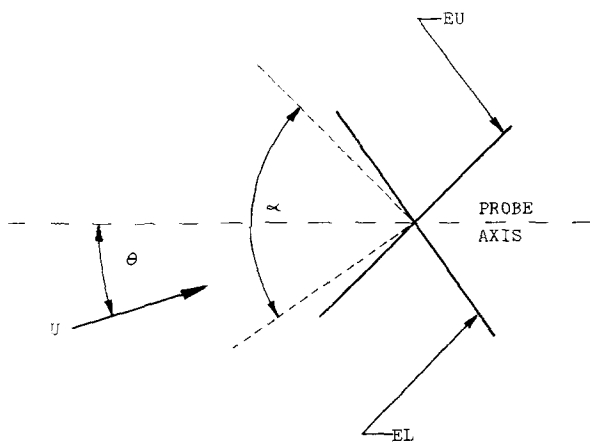

FIG. 15. Geometrical arrangement and symbol definitions for X probe.

The geometry of the probe used for these measurements allowed angles of attack, θ, in the range from $+38°$ to $-51°$. Figure 16 is an example of voltage pairs EL and EU resulting from a typical calibration displayed on the screen of a storage oscilloscope. The points where ambiguity of the voltage pairs was produced by exceeding the range, α, of the probe can be clearly discerned at the edges of the calibration grid. The EL, EU traces appear to curl under producing the same pairs of EL and EU voltages for different pairs of u and v velocity components.

The four tape recorded channels of calibration data were reproduced and digitized with the aid of a Data General Minicomputer System using a 12 bit analog-to-digital converter with simultaneous sample and hold input amplifiers. A computer program was written to process only the unique voltage pairs of calibration data within the range, α, and to construct a relatively coarse (20 $\times$20) calibration table or "grid" with 400 discrete points. The velocity pairs, u and v, and the four partial derivatives of u and v with respect to EL and EU were com-

TABLE I. Properties of the actual and ideal turbulent boundary layer.

	Present work	Coles' ideal boundary layer
U_∞/(m/sec)	9.14	...
Re_θ	11700	11700
δ/cm	17.8	...
δ^*/cm	2.4	...
θ/cm	1.78	...
δ^*/θ	1.349	1.337
u_T/U_∞	0.0350	0.0351
$Re_x/10^{-6}$	3.7	7.9

puted at each of the 400 entry points of the table and stored in the computer.

Measurements were made in a fully turbulent boundary layer with a free stream velocity of 9.1 m/sec. The boundary layer was that developed on the smooth floor of the 1.52×2.13 m wind tunnel at the University of Michigan. The properties of the boundary layer at Re_θ = 11 700 are given in Table I.

Figure 17 shows storage oscilloscope traces of the calibration grids superimposed upon the EL, EU traces produced by the probe when it was immersed in the turbulent boundary layer. In Fig. 17(a), at $y^+ \simeq 650$, the EL, EU traces were all well within the range of values produced during the calibration of the probe. The EL and EU voltages were digitized and stored on magnetic tape. A computer program was used to "look up" and interpolate from the calibration table data the pair of u and v velocity components appropriate for each pair of digitized EL and EU voltages. The results for y^+ greater than approximately 600 ($y/\delta > 0.15$) were in good agreement with those obtained classically in many other investigations. Figures 18 and 19 display the measured values of root-mean square velocities u and v and the Reynolds stress as a function of y. When the probe was nearer the wall, $y/\delta < 0.15$, the measured root-mean-square velocities u and v and also the Reynolds stress were larger than the values measured in classical investigations.

As the probe was moved much closer to the wall, below values of $y^+ = 120$, not only were the root-mean-square velocities u and v and the Reynolds stress too large, but the EL, EU voltage traces obtained in the boundary layer went beyond the valid boundaries of the corresponding calibration grid at that location. Figures 17(b) and 17(c) show typical results at $y^+ \simeq 65$ and at $y^+ \simeq 3$ (the smallest distance from the wall that could be obtained with the small X probe). The EL, EU traces began to exceed the bounds of the calibration grid first on the lower, outflow ($v > 0$) portion of the grid and then also on the upper, inflow ($v < 0$) portion of the grid. The excursions from the grid were characteristically rather intense and rapid voltage fluctuations. As the probe approached the wall the excursions from the grid became more numerous. Very near the wall at $y^+ \simeq 10$ the excursions were so frequent that 19% of the time the voltage pairs were off the grid. Furthermore, 40% of the time that the velocity was lower than the mean and outward from the wall the EL, EU traces were off the grid.

The occurrence of excursions from the calibration grid made it impossible to assign the correct velocity pairs u and v to the voltage pairs EL and EU that were off the grid. Furthermore, even when the voltage pairs were within the calibration grid there is no way to guarantee the accuracy of the assignment of velocity pairs to voltage pairs using the calibration data. Figures 18 and 19 show values of the root-mean-square velocity components of u and v and values of the Reynolds stress $\overline{uv}$ as well as the measurements of these quantities using conventional techniques by Klebanoff,[27] Schubauer[28] and Lu and Willmarth.[29] When the voltage pairs were off the grid, in the present measurements, the velocity pair at the point of departure from the grid was assigned to each voltage pair thereafter until the voltage pairs again returned to the grid. The present data of Figs. 18 and 19 are, therefore, seriously in error near the wall for $y/\delta < 0.15$ or $y^+ < 600$.

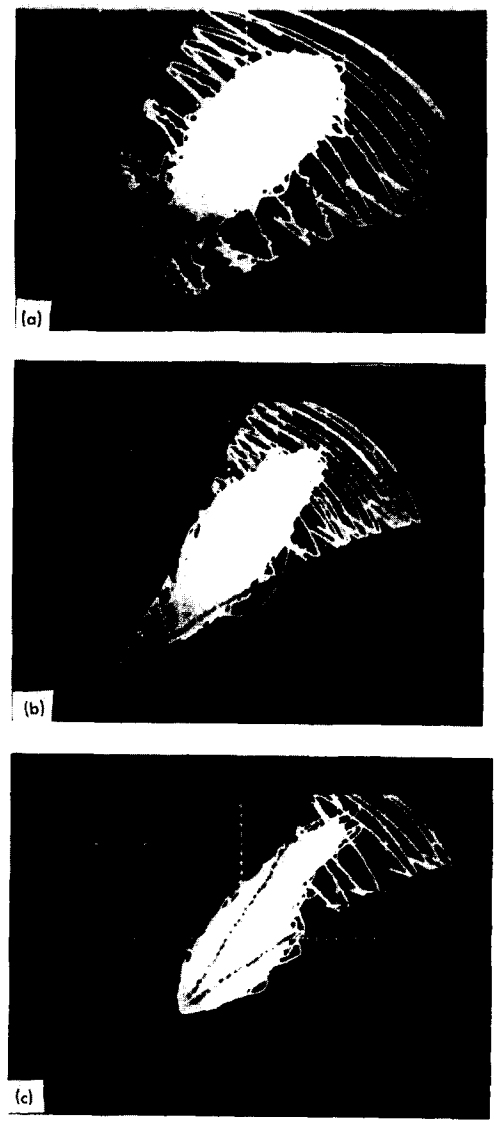

FIG. 17. Photographs of EL and EU voltages during turbulence measurements and calibrations displayed on screen of storage oscillosocpe. (a) $y^+ = 670$; (b) $y^+ = 65$; (c) $y^+ = 3$.

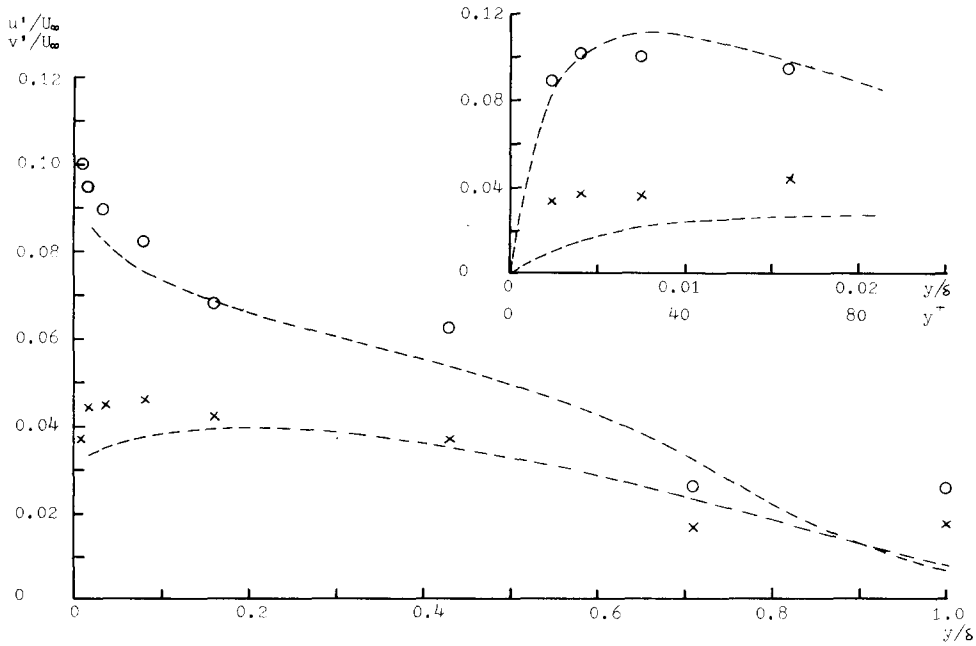

FIG. 18. Profiles of rms velocity fluctuations in the streamwise direction, u', and normal to the wall v'. o, u'/U_∞; ×, v'/U_∞; - - - data of Klebanoff.[27]

A number of hypotheses which might explain the cause of the excursions from the calibration grid include aerodynamic or thermal interaction between the hot wires or their supports, the presence of the transverse velocity component, w, the presence of free convection effects and motion or vibration of the hot wires. A detailed discussion and analysis of the effect that each of these phenomena would have on the EL, EU voltage traces is presented in Bogar.[25] The result of the analysis was that the presence of a transverse velocity acts to bring the EL, EU trace back on the grid. The thermal effects are confined to a wake region which is thin compared with the spacing between the wires, and thus could not cause large excursions from the grid. The effect of transverse velocity and heated wake interactions were checked in the wind tunnel by calibrating a yawed probe. Large differences in the calibration grid were not encountered, and it was concluded that transverse velocities and thermal effects did not cause large excursions from the grid. Free convection effects were negligible at the speeds at which large excursions were observed. Motion of the hot wires under the influence of the local flow in the streamwise and spanwise directions would have similar effects on each wire and would not tend to take the EL, EU traces off the grid. Greater motion of one wire than the other could be caused by local flow normal to the wall, but this would tend to put the EL, EU traces back on the grid. The result was that none of these phenomena were found capable of producing large excursions from the grid similar to those observed when the X array was near the wall. The only remaining explanation for the excursions from the calibration grid is

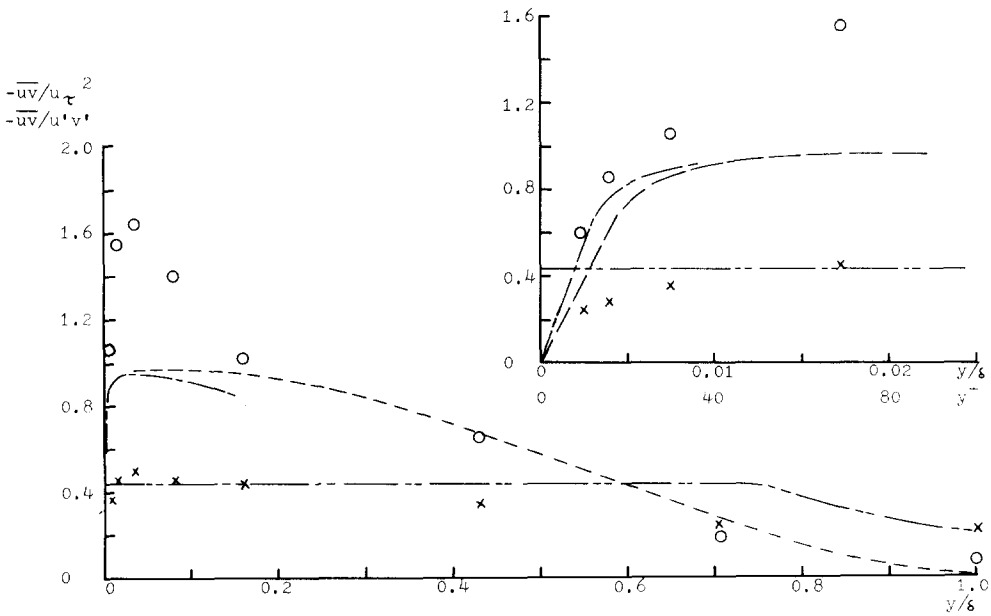

FIG. 19. Profiles of Reynolds stress normalized with rms velocities and wall shear stress. o, $\overline{uv}/u^2$. ×, $\overline{uv}/u'v'$; - - -, data of Klebanoff[27]; — — —, data of Schubauer[28]; —·· —, data of Lu and Willmarth[29]; —·—, profile calculated from mean profile.[25]

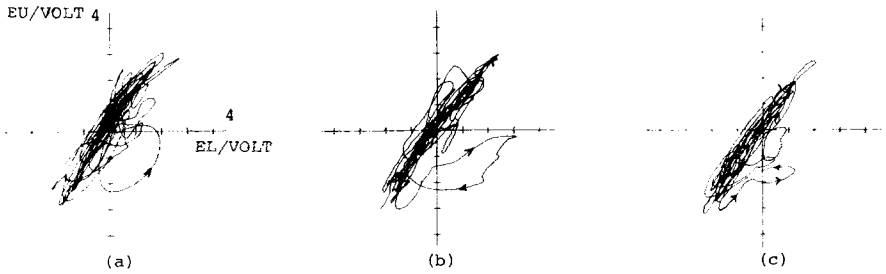

FIG. 20. EL and EU traces of individual high intensity excursions from the calibration grid. (a) $y^+ = 8$; (b), (c) $y^+ = 10$.

that one wire of the array was exposed to flow with a velocity different (in both magnitude and direction) from the velocity to which the other wire in the array was simultaneously exposed. This will occur if the probe encounters severe velocity gradients associated with turbulence of a scale smaller than the probe dimensions. A directly observable example is the two-layer phenomena reported by Corino and Brodkey,[18] see Fig. 5(c), which has a scale less than 20 viscous lengths.

In support of this explanation one should note that during an excursion neither of the voltages EL or EU was one that was not produced during probe calibration. The significant observation is that the *pair* of voltages produced during exposure to the small scale turbulence near the wall was not encountered during calibration of the probe in a uniform flow. Thus, during an excursion one wire of the probe encounters fluid with a velocity different in magnitude and direction from the velocity of the fluid which the other wire encounters. The X array is then not capable of determining the u and v velocity at a point and the excursions from the calibration grid are simply an indication that turbulent structure of a scale smaller than the distance between the hot wires of the X array has been encountered.

The conclusion that is drawn from these results is that the measurements of the root-mean-square velocities $\sqrt{\overline{u^2}}$ and $\sqrt{\overline{v^2}}$ and of the Reynolds stress $\overline{uv}$ for $y^+ < 500$ using a small hot wire X array with 100 μ length, l, ($l^+ = 2.5$) and spacing, s, ($s^+ = 2.5$) are not correct. Thus, the data points shown on Figs. 18 and 19 are in error for $y/\delta < 0.15$ ($y^+ < 500$).

An important question which one must ask is: What does a conventional size X wire array measure in the boundary layer near the wall? For simplicity, let us assume that the wires are very straight, of large aspect ratio, have $\alpha = 90°$, and obey the classical cosine law. Then, one can state that the use of the conventional sum and difference of linearized hot wire output voltages EL and EU to obtain the velocity components u and v will not give correct results when small scale turbulent structures encounter the hot wire array. However, one will not be able to determine when the velocity components u and v determined by the conventional sum and difference technique are in error. Furthermore, since a conventional X array is of the order of ten times as large as the small X array described here much of the effect of the small scale structure will be smeared out by the excessive length of each of the hot wires. This should surpress the excursions from the calibration grid.

To check these conclusions we purchased the smallest commerical available hot wire, X array (Thermosystems Inc. Model 1248T1.5) and calibrated it using the same EL, EU grid technique that was used for our 100

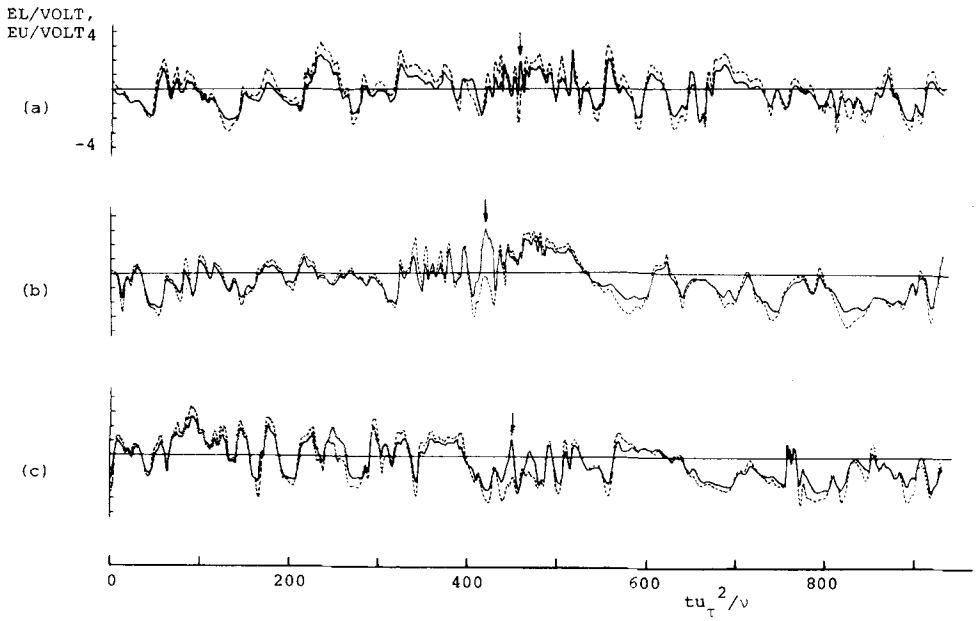

FIG. 21. EL and EU as a function of dimensionless time before and after excursion of Fig. 20. Arrow indicates excursion of Fig. 20. —, EL; ---, EU.

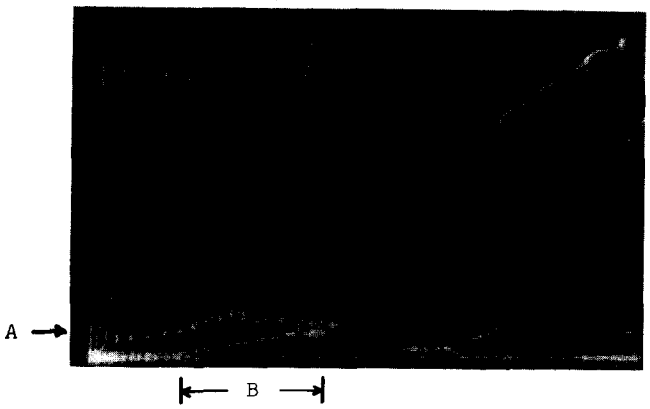

FIG. 22. Growing streamwise vortex near the wall terminating in breakup. Vortex extends from line A over zone B. Note inflectional profile near the normal bubble wire. From Kline *et al.*[17]

μ X array. The wire length, l, was 1200 μ ($l^+ = 30$) and the spacing between the wires, s, was 500 μ ($s^+ = 12.5$). When placed in the boundary layer near the wall, the EL, EU traces were almost always on the grid. However, near the wall with the center of the X array at a distance $y = 800$ μ ($y^+ = 20$) from the wall occasional excursions off the calibration grid were observed. At $y^+ = 20$, only 0.05% of the data pairs EL and EU were off the grid. Furthermore, the excursions were smaller than those measured with the small X array. Although the excursions of the grid were surpressed, the root-mean-square values of the velocity components u and v determined from the calibration grid were 15 to 20% higher than the classical values and the Reynolds stress $\overline{uv}$ was between 50% to 100% higher than the mean shear at the wall for $20 \leq y^+ < 600$.

These results indicate that severe excursions from the calibration grid were suppressed by the spatial averaging of the small scale structure along the length of the larger X array hot wires and by the greater spacing between the wires. They also demonstrate that measurements with conventional X wire arrays are inaccurate when small scale structure is present. Serious measurement errors can occur even if there are no excursions from the calibration grid. This is consistent with the results of measurements of the wall pressure using small transducers, see the results of Bull and Thomas[24] in Fig. 12.

A few of the largest excursions were studied in more detail. Figure 20 shows three examples of large excursions from the calibration grid at points near the wall. Figure 21 shows the corresponding EL and EU traces as a function of time, the location of the beginning of the excursion is marked by an arrow. The interesting feature of this data is that when an excursion occurred a few cycles of high amplitude almost periodic oscillations of the hot wire voltage signals were often observed. This suggests the association of the excursions with small scale oscillatory flow in the region near the wall.

The scale of the velocity gradients responsible for excursions from the calibration grid is much less than the hot wire length or spacing. A rough estimate is that the velocity changes may be small compared with the turbulent velocity fluctuations on a scale of the order of one-tenth of the small hot wire length or spacing. This suggests that velocity changes associated with small scale structure are small relative to the amplitude of turbulent fluctuations over distances of the order of 0.2 viscous lengths (10 μ) or less. The Kolmogoroff length in the boundary layer of Table I is of the order of 170 μ. Therefore, the velocity gradients in the small scale structure near the wall will only become small over a distance that is less than approximately 1/20 of the Kolmogoroff length.

It is important to know more about the nature of the small scale structure near the wall. Our observations suggest that the small scale turbulent flow is energetic and contains definite periodicity when the small scale structure causes excursions of the X array voltage pairs from the calibration grid.

Kim *et al.*[17] have observed intermittent small scale streamwise vortices in bubble traces near the wall. When the vortices occurred, they also observed a few cycles of energetic oscillations of the streamwise velocity. Figure 22 is an example of a bubble trace observed when these oscillations occurred and shows the swirling flow pattern produced by a typical small intense streamwise vortex whose transverse scale is of the order of 2 viscous lengths near its origin. Small scale streamwise vortices were often observed by Kim *et al.*[17] during bursting. We suggest that the streamwise vortical flow structure is primarily responsible for intense small scale gradients in the turbulent flow near the wall.

When drag reduction occurs in practical water flows, the flow speeds are of the order of 1 to 10 m/sec. The transverse scale of the streamwise vortices near the wall is then in the range of 5 μ to 50 μ. We suggest that the size of the small scale flow structures near the wall is comparable to the typical length scale of the shear waves in fluids with polymer additives,[30] or of extended polymer molecules as discussed by Tulin[31] and by Hinch[32] at this symposium. Experiments should be performed that are designed to determine whether or not the development of the small scale vortical structure near the wall is inhibited by polymer additives.

ACKNOWLEDGMENTS

The measurements of streamwise vorticity fluctuations were made at the Max-Planck-Institut fur Strömungforschung, Göttingen, Federal Republic of Germany. The support of the institute and the opportunity to use their facilities is gratefully acknowledged. The experiments with small hot wires were supported by the National Science Foundation and the Office of Naval Research. Their continued assistance over a number of years has made this work possible and is deeply appreciated.

[1]B. A. Toms, in *Proceedings of the 1st International Congress on Rheology* (North Holland, Amsterdam, 1948), Vol. 2, p. 135.

[2]J. L. Lumley, in *Annual Review of Fluid Mechanics*, edited by W. R. Sears and M. Van Dyke (Annual Reviews, Palo Alto, Calif., 1969), Vol. 1, p. 367.

[3]P. S. Virk, E. W. Merril, H. S. Mickley, K.A. Smith, and E. L. Mollo-Christensen, J. Fluid Mech. 30, 305 (1967).
[4]M. J. Rudd, J. Fluid Mech. 51, 673 (1972).
[5]M. M. Reischman and W. G. Tiederman, J. Fluid Mech. 70, 369 (1975).
[6]T. Mizushina and H. Usui, Phys. Fluids 20, S100 (October, Part II, 1977).
[7]L. S. G. Kovasznay, Phys. Fluids Suppl. 10, S25 (1967).
[8]L. S. G. Kovasznay, in *Annual Review of Fluid Mechanics*, edited by M. Van Dyke, W. G. Vincenti, and J. V. Wehausen (Annual Reviews, Palo Alto, Calif., 1970), Vol. 2, p. 95.
[9]E. L. Mollo-Christensen, AIAA J. 9, 1217 (1971).
[10]J. Laufer, in *Instituto Nazionale Di Alta Mathematica*, Symposia Mathematica (Monograf, Bologna, 1972), Vol. IX, p. 299.
[11]W. W. Willmarth, in *Advances in Applied Mechanics*, edited by C. S. Yih (Academic, New York, 1975), Vol. 15, p. 159.
[12]M. J. Lighthill, in *Laminar Boundary Layers*, edited by L. Rosenhead (Oxford University Press, Oxford, 1963), Chap. II.
[13]G. B. Schubauer and P. S. Klebanoff, NACA Report 1289 (1956).
[14]S. Corrsin, in *Naval Hydrodynamics*, Publication 515 (National Academy of Sciences, National Research Council, Washington, D.C., 1957), Chap. XV.
[15]S. J. Kline, W. C. Reynolds, F. A. Schraub, and P. W. Runstalder, J. Fluid Mech. 30, 741 (1967).
[16]A. K. Gupta, J. Laufer, and R. E. Kaplan, J. Fluid Mech. 50, 493 (1971).
[17]H. T. Kim, S. J. Kline, and W. C. Reynolds, J. Fluid Mech. 50, 133 (1971).
[18]E. R. Corino and R. S. Brodkey, J. Fluid Mech. 37, 1 (1969).
[19]G. R. Offen and S. J. Kline, J. Fluid Mech. 62, 233 (1974).
[20]T. Theodorsen, 50 *Jahre Grenzschichtforschung*, edited by H. Görtler and W. Tollmien (Vieweg, Braunschweig, 1955), p. 55.
[21]W. W. Willmarth and B. J. Tu, Phys. Fluids Suppl. 10, S134 (1967).
[22]L. Kastrinakis, J. M. Wallace, and W. W. Willmarth, Bull. Am. Phys. Soc. 20, 1422 (1975).
[23]R. Emmerling, G. E. A. Meier, and A. Dinkelacker, in *AGARD Conference Proceedings* 131 *on Noise Mechanism*, (Advisory Group for Aerospace Research and Development, North Atlantic Treaty Organization, Paris, 1973), paper No. 24; see also A. Dinkelacker, M. Hessel, G. E. A. Meier, and G. Schewe, Phys. Fluids 20, S216 (October, Part II, 1977).
[24]M. K. Bull and A. S. W. Thomas, Phys. Fluids 19, 597 (1976).
[25]T. J. Bogar, Ph.D. thesis, University of Michigan (1975).
[26]J. C. Wyngaard and J. L. Lumley, J. Sci. Instrum. 44, 363 (1967).
[27]P. S. Klebanoff, NACA Technical Note 3178 (1954).
[28]G. B. Schubauer, J. Appl. Phys. 25, 188 (1954).
[29]S. S. Lu and W. W. Willmarth, J. Fluid Mech. 60, 481 (1973).
[30]M. Tulin, Bull. Am. Phys. Soc. 10, 267 (1965).
[31]M. Tulin, in *Sixth Symposium on Naval Hydrodynamics* (Government Printing Office, Washington, D.C., 1966), p. 3.
[32]E. J. Hinch, Phys. Fluids 20, S22 (October, Part II, 1977).